nature nanotechnology

ARTICLES

PUBLISHED ONLINE: 27 FEBRUARY 2017 | DOI: 10.1038/NNANO.2017.17

Triboelectric nanogenerators for sensitive nano-coulomb molecular mass spectrometry

Anyin Li[1†], Yunlong Zi[2†], Hengyu Guo[2], Zhong Lin Wang[2,3*] and Facundo M. Fernández[1,4*]

Ion sources for molecular mass spectrometry are usually driven by direct current power supplies with no user control over the total charges generated. Here, we show that the output of triboelectric nanogenerators (TENGs) can quantitatively control the total ionization charges in mass spectrometry. The high output voltage of TENGs can generate single- or alternating-polarity ion pulses, and is ideal for inducing nanoelectrospray ionization (nanoESI) and plasma discharge ionization. For a given nanoESI emitter, accurately controlled ion pulses ranging from 1.0 to 5.5 nC were delivered with an onset charge of 1.0 nC. Spray pulses can be generated at a high frequency of 17 Hz (60 ms in period) and the pulse duration is adjustable on-demand between 60 ms and 5.5 s. Highly sensitive (~0.6 zeptomole) mass spectrometry analysis using minimal sample (18 pl per pulse) was achieved with a 10 pg ml^{-1} cocaine sample. We also show that native protein conformation is conserved in TENG-ESI, and that patterned ion deposition on conductive and insulating surfaces is possible.

Owing to its high sensitivity and unsurpassed molecular specificity, mass spectrometry (MS) is a key analytical tool with applications in biomedicine, food science, homeland security, systems biology, drug discovery and other fields[1]. The voltage applied to the ion source serves as one of the benchmark parameters for the process of converting neutral species into gas-phase ions prior to mass analysis. However, the number of generated ions does not depend on the applied voltage in a straightforward fashion. As a result, controlling the number of charges used in the ionization of neutral species is typically impossible. Moreover, a large portion of the d.c. current—and therefore ions—is wasted due to the pulsed, low duty cycle nature of ion traps[2], ion mobility[3,4], Fourier transform[5,6], charge detection[7], and other advanced ion analysis systems[8]. As a result, ions are typically generated at currents ranging from nA to μA, but only pA levels reach the mass analyser. All these complications strongly affect sample utilization efficiency, limits of detection, quantitative performance and duty cycle. Conventional high-voltage power supplies used for powering ion sources also suffer from disadvantages such as high cost, limited portability and safety concerns. Specialized electronic components such as high-voltage switches and transformers are required in more elaborate electrospray ionization (ESI) modes driven by high-voltage pulses[9–11], dielectric barrier polarization[12], or capacitive induction[13]. The recent demonstration that charge pulses can trigger ESI[14] has opened the path for developing simpler and more robust devices with fine and reproducible control of the ionization process.

TENGs are sustainable power sources that convert ambient mechanical motion into electricity[15–17]. Integrated into self-powered systems, TENGs have shown great potential in biomedical science and personal electronics[18,19]. Based on triboelectrification[20,21] and electrostatic induction, TENGs generate electric energy through a fixed number of charges that are proportional to the surface area of the functional material, typically in the tens to hundreds of μC m^{-2} per cycle[16], with stability tested up to 10 million cycles with minimal degradation[22–24]. This quantized charge generation in the nC range is beyond the reach of conventional power supplies, and may provide a simple solution for charge-quantity-controlled ion generation in mass-to-charge or ion mobility-based analysis.

Here, we report the first set of TENG-driven ion sources for mass spectrometric analysis. Both nanoESI and plasma discharge ionization were successfully achieved. The fixed number of charges provided by TENGs offered unprecedented control over ion generation. With a rationalized physics model, controllable ion generation with nC accuracy was demonstrated. The duration, frequency and polarity of generated ion pulses were all controllable via TENG actuation on-demand, with minimum sample consumption. The high voltage (5–9 kV) of TENGs provided nanoESI with enhanced sensitivity at low concentrations, while the small number of charges in each ion pulse maximized sample utilization. A wide range of chemical compounds, ranging from small organic molecules, such as explosives and chemical warfare simulants, to large biomolecules were all successfully investigated by TENG MS. Alternating-polarity electrospray pulses triggered by TENGs were also demonstrated to deposit materials in patterns onto both conductive and insulating surfaces.

Design and characterization of nC ionization source

TENGs are composed of two electrodes and at least one pair of triboelectric layers. The mechanical movement of these layers with respect to each other breaks the original electrostatic balance and induces charge redistribution in the electrodes, leading to charge output through the connected external circuit. Figure 1 illustrates the contact-separation (CS) and sliding freestanding (SF) TENGs used in this work, and their coupling to a nanoESI emitter. The CS-TENG (Fig. 1a) and SF-TENG (Fig. 1b) were used to generate single-polarity and alternating-polarity charge pulses, respectively (Supplementary Note 1). A motion-triggered switch (S_C) was mounted on the side of the CS-TENG to reset the electrostatic

[1]School of Chemistry and Biochemistry, Georgia Institute of Technology, Atlanta, Georgia 30332, USA. [2]School of Materials Science and Engineering, Georgia Institute of Technology, Atlanta, Georgia 30332, USA. [3]Beijing Institute of Nanoenergy and Nanosystems, Chinese Academy of Sciences, National Center for Nanoscience and Technology (NCNST), Beijing 100083, China. [4]Institute of Bioengineering and Biosciences, Georgia Institute of Technology, Atlanta, Georgia 30332, USA. †These authors contributed equally to this work. *e-mail: facundo.fernandez@chemistry.gatech.edu; zhong.wang@mse.gatech.edu

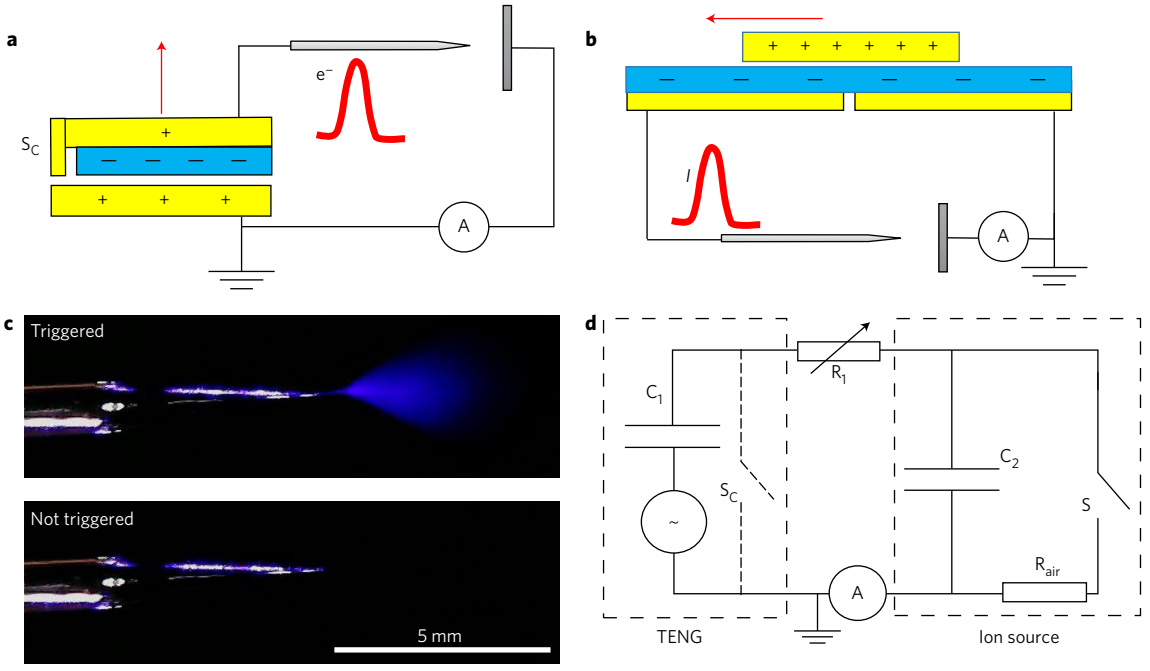

Figure 1 | Ionization by TENGs. a,**b**, Schemes showing the mechanism of contact-separation (CS; **a**) and sliding freestanding (SF; **b**) mode TENGs. Yellow, copper electrode layers; blue, fluorinated ethylene propylene layers. The red arrows and pulses denote moving directions of the TENG electrodes and the corresponding charge flow (e^-, I) to the ion source, such as the nanoelectrospray emitter represented by the needle shape. The vertical rectangle represents a steel plate collecting the ion current, which is measured by a picoamperemeter (represented by the A symbol). **c**, Dark-field images of a nanoelectrospray emitter showing an electrospray plume triggered by the TENG charge flow. **d**, In an equivalent electronic circuit, the TENG is symbolized by a capacitor (C_1) together with the components in the dashed rectangle on the left; the nanoESI emitter is equivalent to a capacitor (C_2) that would leak (S) after reaching an onset charge value, represented by the components within the dashed rectangle on the right. The leaked charges (that is, generated ions) fly through the air gap (R_{air}) between the emitter and the mass spectrometer or picoamperemeter (A). Note that the CS-TENG electrodes (**a**) are extended on the side to reset the electrostatic status at the contact position, represented as switch S_C in **d**.

status at the time of contact of the triboelectric layers for single-polarity charge pulse generation[25]. The generated charges were supplied to a nanoESI emitter (Fig. 1c), or to a needle electrode for plasma discharge ionization. In the equivalent circuit (Fig. 1d), the ion source is described as equivalent to a capacitor (C) that would leak (symbolized as a switch, S) through air (R_{air}) when its voltage is larger than the onset value. Each TENG cycle would thus result in one leak event, that is, one ionization pulse. The 'leaked' ions can be measured by an electrometer (A), or analysed by a mass spectrometer.

The observation of TENG-triggered electrospray droplet generation (Fig. 1c) indicated the ~1 kV onset voltage of the nanoESI emitter was reached. Figure 2a shows the voltage–charge (V–Q) plot[26] of a TENG while charging an ion source ($C_{\text{ion Source}}$). A small amount of charge is consumed by the nanoESI emitter before reaching its onset voltage (V_{onset}). After this onset voltage is reached, the triggered electrospray releases a number of charges (Fig. 2a, green line) until the TENG voltage drops below the onset voltage. The discrete amount of available charge from the TENG ensures highly repeatable ionization pulses, as shown by the charge versus time plot in Fig. 2b. Compared with the stochastic pulses in conventional pulsating ESI modes[27], which are achieved by applying a d.c. voltage slightly above the onset voltage[28], the much higher open-circuit voltage (V_{OC}) values achieved with TENGs (Supplementary Figs 1–3, Supplementary Note 2 and Supplementary Tables 1–3) generated spray pulses in the cone-jet mode[28], following each on-demand actuation.

Control over total charge number, polarity and frequency

Quantitative control over the amount of generated ions, that is, Q_{pulse}, can be achieved by varying the output of the TENG or varying the onset voltage of the ion source, as illustrated qualitatively by the physics model in Fig. 2a. For a specific set-up with a given TENG and emitter, a resistor (R_1 in Fig. 1d) was used to reduce the effective voltage applied to the ion source. This was equivalent to increasing V_{onset}, leading to a decrease in Q_{pulse}, as explained in detail in Supplementary Fig. 4. Spray pulses of 1.0, 2.8, 3.5 and 5.5 nC, shown in Fig. 2b, were generated using 1.25, 1, 0.5 GΩ and 0 (no) resistors, respectively. At the onset spray condition, corresponding to ~1 nC onset charge, successful spraying and unsuccessful meniscus 'rippling' (Fig. 2b inset and Supplementary Fig. 2a) occurred with equal probabilities. The capacitance of the nanoESI emitter was estimated using the magnitude of the rippling charge as the lowest possible value and the sprayed charge amount as the highest possible value. Divided by the onset voltage of 1,000 V, a capacitance of 0.3–1 pF was estimated for an emitter with 2-μm inner-diameter tip. Similarly, a larger emitter with 20-μm tip diameter and 1,600 V onset voltage showed a capacitance of 0.3–2.5 pF (Supplementary Fig. 2). In comparison, the measured capacitance for the voltmeter is 301 pF (Supplementary Fig. 5).

Besides controlling the amount of charge available for ionization, mechanically driven TENGs can also control the duration, polarity and frequency of the downstream ion signal. With a CS-TENG, all charges are generated simultaneously at the transient moment when the two triboelectric layers separate. As a result, the generated nanoESI pulse duration was determined by the available charges above the onset voltage, which cannot be easily varied without changing the device dimensions. In comparison, SF-TENGs generate charges progressively as the two surfaces slide. This feature was utilized to achieve either longer spray pulses by slow sliding motion, or higher-frequency spray pulses by rapidly switching the

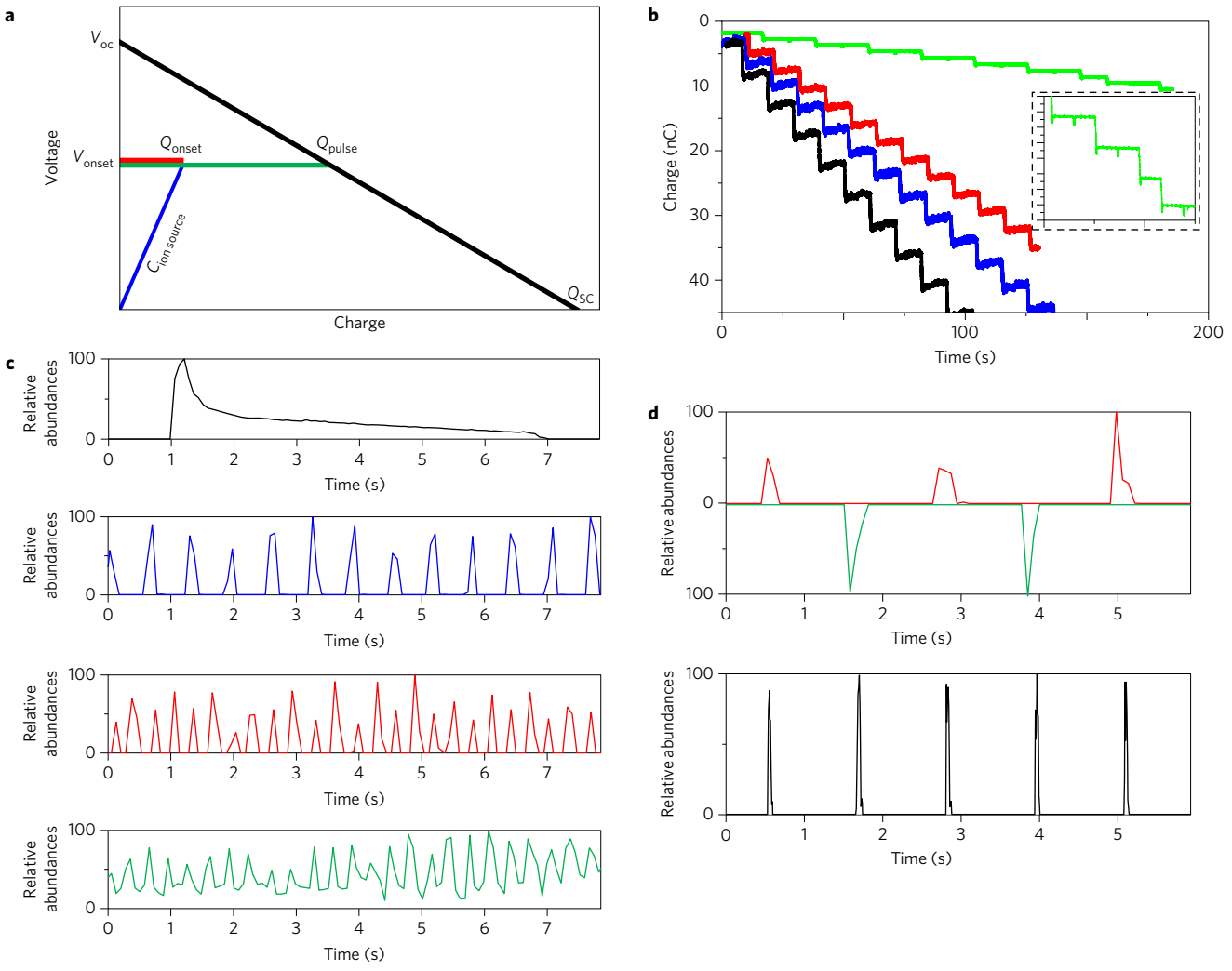

Figure 2 | TENG accurately controls nanoelectrospray ionization. a, Scheme representing how a TENG charges an ion source. The V_{OC}–Q_{SC} line represents the TENG's voltage after supplying a certain amount of charge. When a nanoESI emitter was connected, charges were delivered to this ion source ($C_{ion\ source}$) until an onset voltage (V_{onset}) was reached immediately prior to ionization. Then, a number of charges were released in the form of electrospray ionization, represented by the green line Q_{pulse}, until the TENG voltage drops below the onset. **b**, Time–charge plots describing the ionization pulses from one CS-TENG-driven nanoESI emitter. The four traces are the results of using different resistances: 0 (black), 0.5 (blue), 1 (red) and 1.25 (green) GΩ, in series to regulate the delivered charge. The green trace, magnified in the inset, corresponded to an onset condition when ~50% of the actuation events did not successfully generate electrospray. Instead, a small dip was observed corresponding to capacitive charging and discharging. **c**, Total ion chronograms of long duration and shorter, high-frequency pulses generated on-demand: >5 s (black), 600 ms (blue), 300 ms (red) and 60 ms (green), using the SF-TENG. **d**, Total ion chronogram for alternating-polarity spray pulses (red and green) in one experiment and rectified single-polarity pulses (black) in another experiment. In all cases above, a methanol:water (1:1) solution was used for testing purposes.

direction of the sliding motion without delay. As shown in Fig. 2c, spray pulses ranging from >5 s per spray to <75 ms per spray were recorded by the mass spectrometer. When the frequency of the spray pulses was faster than the sampling interval (75 ms) of the mass spectrometer, a pseudo-continuous total ion chronogram was observed (Fig. 2c-green trace). A salient feature of SF-TENGs is the generation of alternating-polarity spray pulses (Fig. 2d), which is an established strategy for increasing analyte coverage in both ultra-high-performance liquid chromatography (UHPLC)–MS analysis[29] and MS imaging[30]. When single-polarity spray pulses (Fig. 2d) were desired from an SF-TENG, a diode bridge was implemented.

Analytical advantages

In all cases, pulsed electrospray ion signals were generated with high reproducibility due to the discrete amount of charge output by the TENGs. In a typical experiment where the mass spectrometer sampling frequency is higher than that of the pulse generation, the relative standard deviation (RSD) of the total ion chronogram signals was only 3% ($n = 10$, Supplementary Fig. 6). At micromolar concentrations, various analytes were ionized by TENG-nanoESI MS with sensitivity similar to that obtained using conventional nanoESI. However, as concentrations approached the limits of detection (LOD), TENG-nanoESI outperformed standard nanoESI. For example, when analysing a very dilute 10 pg ml^{-1} cocaine sample under parallel reaction monitoring mode ($m/z = 182$ as the precursor ion), standard d.c. (1–2 kV) nanoESI did not generate any detectable signature fragment ions. In comparison, the SF-TENG (V_{OC}, 5–9 kV) nanoESI produced a detectable signal at the same concentration level, using the same nanoESI emitter (Fig. 3). If the CS-TENG (V_{OC}, 1.6 kV) was used, no fragment ion signal was observed. This sensitivity enhancement is believed to be a result of the higher (5–9 kV) V_{OC} of the SF-TENG as compared with the CS-TENG and standard nanoESI. It is worth noting that if a d.c. voltage in the 5–9 kV range were to

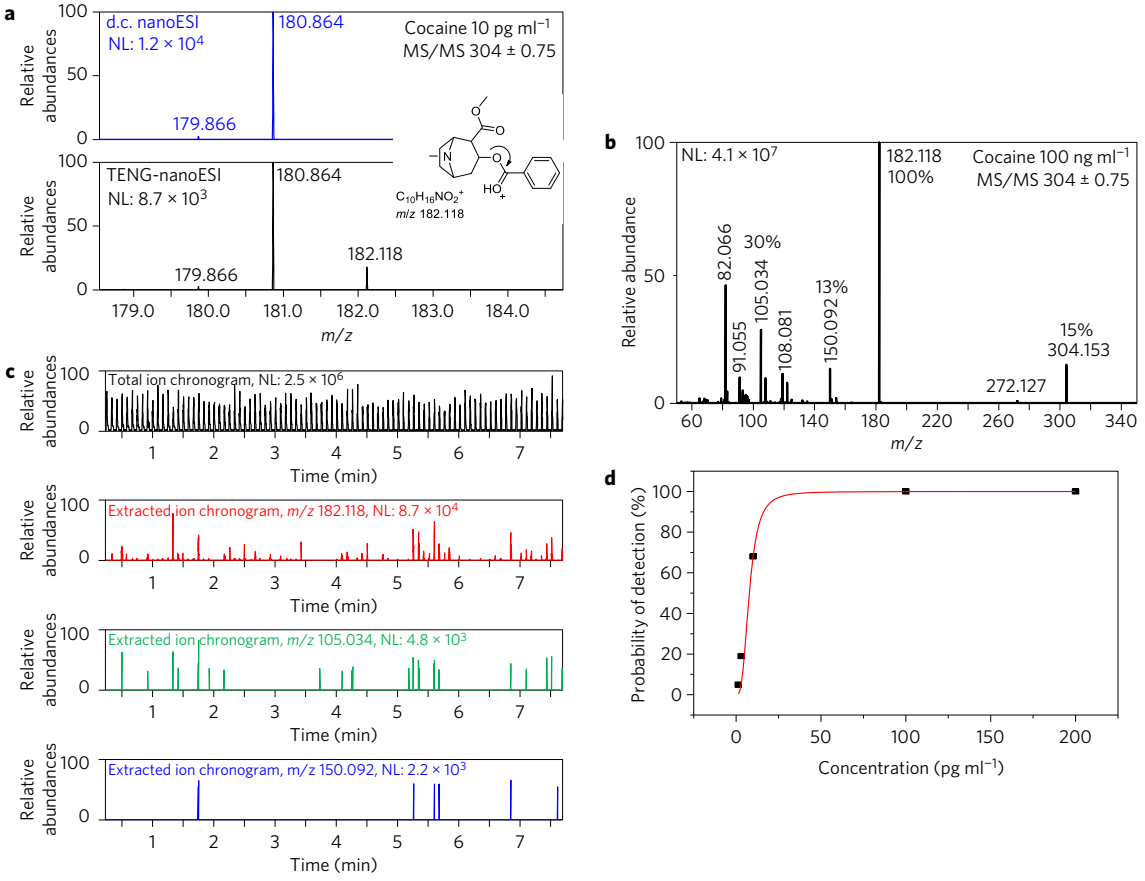

Figure 3 | Enhanced sensitivity under transient TENG high voltage. a, Signature fragment ion (*m/z* 182.118) can only be observed by the SF-TENG when analysing a cocaine solution (10 pg ml^{-1}) in positive-mode nanoESI MS/MS. **b**, In the fragmentation pattern, protonated cocaine cation observed under a higher (100 ng ml^{-1}) concentration. The relative abundances of four signature fragment ions are labelled. **c**, Mass analysing consecutive SF-TENG nanoESI pulses for a 10 pg ml^{-1} cocaine solution under MS/MS mode. The extracted ion chronograms of the fragment ions with lower relative abundances (**b**), show a decreasing probability of detection (POD). All the peaks in (**a**–**c**) were normalized according to the base peaks, whose absolute intensities were labelled as the normalized levels (NL). **d**, The POD values (symbols) fitted to a logistic function (red line) so that detection limits can be calculated.

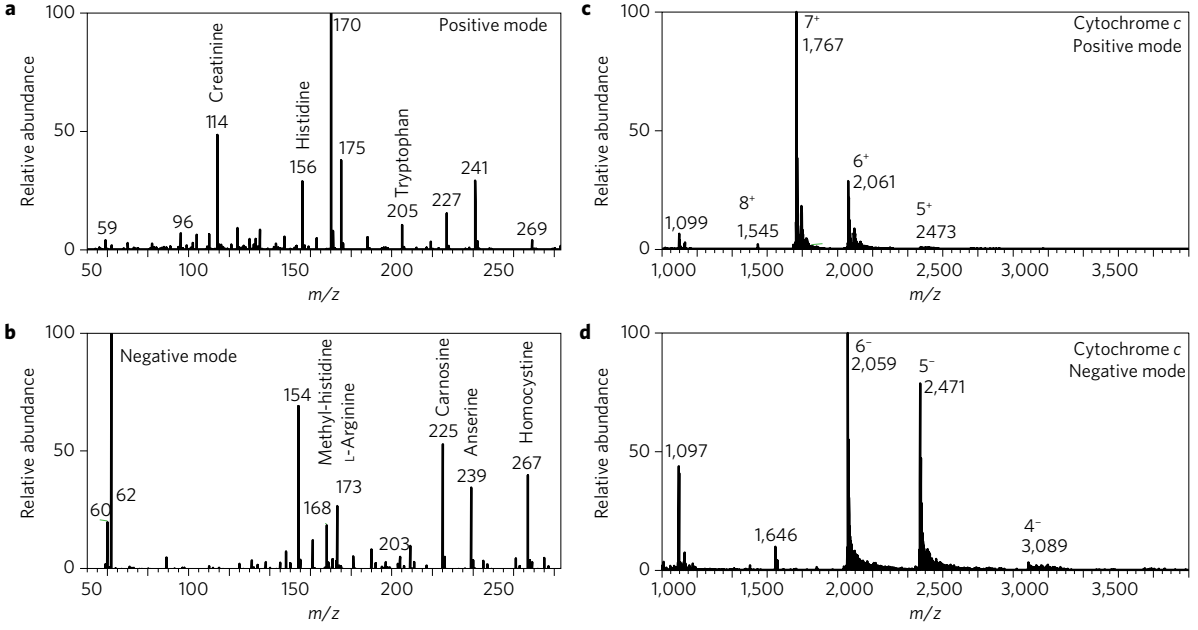

Figure 4 | Dual-polarity ionization and preservation of native biomolecule conformation. a,**b**, A mixture containing creatinine, histidine, methyl-histidine, arginine, tryptophan, carnosine, anserine and homocysteine, each at 2.5 μM, ionized to $[M + H]^+$ and $[M - H]^-$ species in alternating pulses by the SF-TENG. **c**,**d**, 10 μM cytochrome *c* in an aqueous 100 mM ammonium acetate aqueous solution, subject to the alternating SF-TENG. The prevailing charge states of the cytochrome *c* ions indicates native solution phase conformations are conserved.

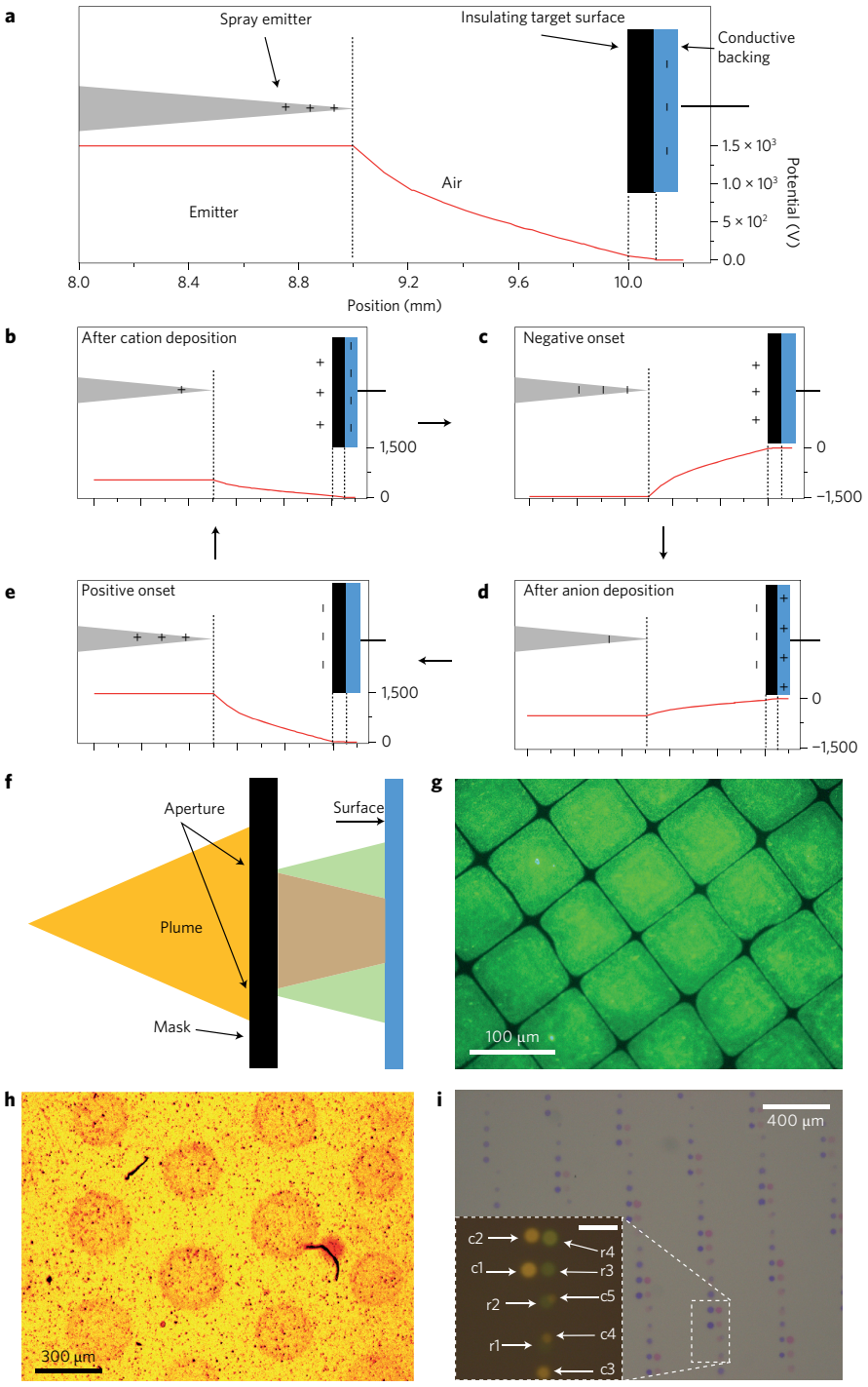

Figure 5 | Ion deposition on various types of surface using the SF-TENG. a, Components in the deposition apparatus. The electric potentials are simulated using COMSOL Multiphysics, details in Supplementary Table 4. **b**, Immediately before deposition the positive charges accumulate on the emitter tip. **c**, After the first positive spray pulse is deposited onto the insulating surface, the electric potential at the surface rises and there is not enough charge at the emitter so the spray deposition stops. **d**, Then, the polarity of the emitter cycles due to the SF-TENG action. An opposite electric gradient is established, triggering a spray pulse of the opposite polarity that neutralizes the surface charge, and deposits the solute. **e**, After depositing negative charges on the surface, the spray stops, similar to **c**. Then the polarity of the emitter is switched again, cycling back to **b**, and releasing the next spray pulse. **f**, Scheme showing that the charged spray plume (yellow), after passing through the mask aperture, was focused (brown) with grounded conducting target surfaces, or defocused (green) with insulating target surfaces. **g**, An array of Alexa Fluor 488 fluorescent squares was deposited on an insulating glass cover slide, using a transmission electron microscopy grid as the mask. **h**, On an insulating polyimide tape, the deposited patterned crystal violet spots (~300 μm) were larger than the mask aperture (~200 μm) as a result of the defocusing effect. The other smaller visible features are air bubbles and dust particles trapped in the adhesive layer of the tape. **i**, On a conductive grounded indium tin oxide slide, obtained spots were smaller than the aperture. The spots shown in the regions highlighted by the dashed rectangle were created sequentially by moving the target surface and using crystal violet and Rhodamine 6G solutions. The dark-field image in the inset illustrates the decreasing spot sizes (c1–c5, 50–15 μm) obtained by increasing mask-to-surface distance from 50 to 300 μm in 50 μm steps. Also shown are spots with different amounts of material generated by spraying Rhodamine 6G (r1–r4), and varying the number of spray pulses from 50 to 200 in 50 pulse steps. The scale bar in the inset is 100 μm.

be applied to the nanoESI emitter via a standard power supply, the emitter would be permanently damaged by the ensuing corona discharge, which was typically observed at an onset voltage of 2–2.5 kV. Similar sensitivity enhancements were observed with peptide analytes in the negative ion mode (Supplementary Fig. 7). Long-term sample consumption experiments showed that 13.7 nl of cocaine sample (10 pg ml^{-1}) loaded in the nanoESI emitter (Supplementary Fig. 8) were exhausted in 748 spray pulses, each lasting 1.60 ± 0.05 s on average. This corresponded to a consumption rate of 18 pl per spray pulse, and an average flow rate of 11 pl s^{-1}. Each spray pulse was thus equivalent to ~0.6 zeptomole (~360 molecules) for the 10 pg ml^{-1} cocaine solution tested.

Parallel reaction monitoring MS experiments essentially result in no 'noise' at m/z 182.118 in the absence of analyte ions (Supplementary Fig. 9), therefore making signal-to-noise ratio LOD estimation impossible. To accurately estimate LODs, a probability of detection strategy[31] was adopted. Figure 3c shows the decreasing frequency of detection for fragment ions with decreasing abundances, ranging from 13% to 68% for fragments at m/z 182.118, 105.034 and 150.092. For the m/z 182.118 fragment ion, the cocaine concentrations corresponding to 50% and 95% probability of detection were 8 pg ml^{-1} (0.5 zmol) and 21 pg ml^{-1} (1.3 zmol), respectively (Fig. 3d). Further enhancements to these figures of merit could be achieved by synchronizing the TENG actuation event with the mass analysis (pulsing or trapping) events.

When coupling the ability of the SF-TENG nanoESI MS to generate both positive and negative ions via alternating-polarity sprays with a polarity-switching MS mode, two sets of information were obtained in one interleaved experiment, as demonstrated for the analysis of amino acid mixtures and protein samples (Fig. 4). For proteins, solution-phase conformation was still preserved when using the high V_{OC} SF-TENG. As shown in Fig. 4c,d, cytochrome c primarily produced 6^+ and 7^+ charge states in positive mode, and 4^-, 5^- and 6^- charge states in negative mode, corresponding to native conformations[32]. Besides proteins, other biomolecule classes such as DNA were also readily ionized from aqueous solutions (Supplementary Fig. 10). Destructive corona discharge, an issue in the electrospray of aqueous or other high-surface-tension solutions under high voltage[33], was never observed in any of the ESI experiments using CS-TENGs and SF-TENGs with short-circuit charge transfers (Q_{SC}) of ~120 nC and ~140 nC, respectively (Supplementary Fig. 1). This result agrees with the experimental fact that a sharp stainless steel needle that is placed at the same distance (5 mm) from the mass spectrometer inlet and connected to the same SF-TENG, created no corona discharge, which is detrimental for nanoESI, but useful in atmospheric pressure chemical ionization for the analysis of small drug molecules, narcotics, explosives and toxic chemicals[34]. Using an SF-TENG with Q_{SC} of ~140 nC, a stainless steel needle, and a needle-to-inlet distance of 1.5 mm resulted in plasma discharge ion signals that were highly repeatable, with a peak area RSD of 7% (Supplementary Fig. 11). Ionization of a variety of target compounds, such as dimethyl methylphosphonate (DMMP), hexylamine and trinitrotoluene (TNT), was readily achieved in either positive or negative mode via this plasma (Supplementary Figs 12 and 13).

Applications in materials science

Besides mass spectrometric analysis, ion beams and charged droplets also play important roles in material fabrication and surface modification[35–37]. Delivery of specific compounds to desired surface locations under atmospheric pressure enables advanced capabilities such as those required in microarray assays[38] and functional surfaces[39]. Using SF-TENGs, sheathless electrospray deposition onto both conductive and insulating surfaces was achieved using on-demand alternating-polarity discrete charged packets. Generally, electrospray deposition onto insulating surfaces is hampered by charge repulsion effects. Neutralization strategies, such as rotating the surface between a single-polarity spray and a reverse-polarity corona discharge, have been adopted to achieve continuous deposition[40]. Using SF-TENG-driven nanoESI, alternating-polarity spray pulses were deposited on insulating surfaces in a layer-by-layer fashion (Fig. 5a–e). As an example, a square pattern was deposited on an insulating glass cover slide (Fig. 5g). A defocusing effect (Fig. 5f) was observed when depositing ions onto insulating surfaces through the apertures of a mask (Fig. 5g,h). This defocusing effect is opposite to the mask's focusing effect when faced with grounded surfaces[41] (Fig. 5i), and is consistent with the expansion effect that accompanies ion deceleration in ion optics.

Conclusions

We demonstrated ion generation by discrete amount of charges enabled by the high output voltage of a TENG. Both electrospray ionization and plasma discharge ionization were achieved. Unprecedented control over the ionization process was enabled by quantized ion pulses of adjustable duration, polarity and frequency. For electrospray ionization, a physics model was developed to explain the number of charges in each ionization pulse. This opens the door for using charge numbers as a new parameter, in addition to sample concentration, flow rate, and so on, for quantitative MS analysis. These new capabilities provide rich avenues for addressing future challenges in chemical and biochemical detection. TENG-driven ionization represents a simple, safe and effective approach, opening the possibility for efficient ionization with accurate numbers of total charges.

Methods

Methods and any associated references are available in the online version of the paper.

Received 14 July 2016; accepted 26 January 2017;
published online 27 February 2017

References

1. Maher, S., Jjunju, F. P. M. & Taylor, S. Colloquium: 100 years of mass spectrometry: perspectives and future trends. *Rev. Mod. Phys.* **87,** 113–135 (2015).
2. Louris, J. N. *et al.* Instrumentation, applications, and energy deposition in quadrupole ion-trap tandem mass-spectrometry. *Anal. Chem.* **59,** 1677–1685 (1987).
3. Bohrer, B. C., Mererbloom, S. I., Koeniger, S. L., Hilderbrand, A. E. & Clemmer, D. E. Biomolecule analysis by ion mobility spectrometry. *Annu. Rev. Anal. Chem.* **1,** 293–327 (2008).
4. Ruotolo, B. T., Benesch, J. L. P., Sandercock, A. M., Hyung, S. J. & Robinson, C. V. Ion mobility-mass spectrometry analysis of large protein complexes. *Nat. Protoc.* **3,** 1139–1152 (2008).
5. Gross, M. L. & Rempel, D. L. Fourier transform mass spectrometry. *Science* **226,** 261–268 (1984).
6. Hu, Q. Z. *et al.* The orbitrap: a new mass spectrometer. *J. Mass Spectrom.* **40,** 430–443 (2005).
7. Contino, N. C., Pierson, E. E., Keifer, D. Z. & Jarrold, M. F. Charge detection mass spectrometry with resolved charge states. *J. Am. Soc. Mass Spectrom.* **24,** 101–108 (2013).
8. Webb, I. K. *et al.* Mobility-resolved ion selection in uniform drift field ion mobility spectrometry/mass spectrometry: dynamic switching in structures for lossless ion manipulations. *Anal. Chem.* **86,** 9632–9637 (2014).
9. Liang, X. R., Han, H. L., Xia, Y. & McLuckey, S. A. A pulsed triple ionization source for sequential ion/ion reactions in an electrodynamic ion trap. *J. Am. Soc. Mass Spectrom.* **18,** 369–376 (2007).
10. Bushey, J. M., Kaplan, D. A., Danell, R. M. & Glish, G. L. Pulsed nano-electrospray ionization: characterization of temporal response and implementation with a flared inlet capillary. *Instrum. Sci. Technol.* **37,** 257–273 (2009).
11. Xu, W., Charipar, N., Kirleis, M. A., Xia, Y. & Ouyang, Z. Study of discontinuous atmospheric pressure interfaces for mass spectrometry instrumentation development. *Anal. Chem.* **82,** 6584–6592 (2010).
12. Schilling, M., Janasek, D. & Franzke, J. Electrospray-ionization driven by dielectric polarization. *Anal. Bioanal. Chem.* **391,** 555–561 (2008).
13. Huang, G. M., Li, G. T. & Cooks, R. G. Induced nanoelectrospray ionization for matrix-tolerant and high-throughput mass spectrometry. *Angew. Chem. Int. Ed.* **50,** 9907–9910 (2011).

14. Li, A., Hollerbach, A., Luo, Q. & Cooks, R. G. On-demand ambient ionization of picoliter samples using charge pulses. *Angew. Chem. Int. Ed.* **54,** 6893–6895 (2015).
15. Wang, Z. L. Triboelectric nanogenerators as new energy technology for self-powered systems and as active mechanical and chemical sensors. *ACS Nano* **7,** 9533–9557 (2013).
16. Wang, Z. L., Chen, J. & Lin, L. Progress in triboelectric nanogenerators as a new energy technology and self-powered sensors. *Energy Environ. Sci.* **8,** 2250–2282 (2015).
17. Wang, Z. L. Triboelectric nanogenerators as new energy technology and self-powered sensors - principles, problems and perspectives. *Faraday Discuss.* **176,** 447–458 (2014).
18. Tang, W. *et al.* Implantable self-powered low-level laser cure system for mouse embryonic osteoblasts proliferation and differentiation. *ACS Nano* **9,** 7867–7873 (2015).
19. Niu, S. M., Wang, X. F., Yi, F., Zhou, Y. S. & Wang, Z. L. A universal self-charging system driven by random biomechanical energy for sustainable operation of mobile electronics. *Nat. Commun.* **6,** 8795 (2015).
20. McCarty, L. S. & Whitesides, G. M. Electrostatic charging due to separation of ions at interfaces: contact electrification of ionic electrets. *Angew. Chem. Int. Ed.* **47,** 2188–2207 (2008).
21. Baytekin, H. T. *et al.* The mosaic of surface charge in contact electrification. *Science* **333,** 308–312 (2011).
22. Wang, S. *et al.* Molecular surface functionalization to enhance the power output of triboelectric nanogenerators. *J. Mater. Chem. A* **4,** 3728–3734 (2016).
23. Zhu, G., Chen, J., Zhang, T. J., Jing, Q. S. & Wang, Z. L. Radial-arrayed rotary electrification for high performance triboelectric generator. *Nat. Commun.* **5,** 3426 (2014).
24. Chen, J. *et al.* Harmonic-resonator-based triboelectric nanogenerator as a sustainable power source and a self-powered active vibration sensor. *Adv. Mater.* **25,** 6094–6099 (2013).
25. Zi, Y. *et al.* Effective energy storage from a triboelectric nanogenerator. *Nat. Commun.* **7,** 10987 (2016).
26. Zi, Y. *et al.* Standards and figure-of-merits for quantifying the performance of triboelectric nanogenerators. *Nat. Commun.* **6,** 8376 (2015).
27. Wei, Z. *et al.* Pulsed direct current electrospray: enabling systematic analysis of small volume sample by boosting sample economy. *Anal. Chem.* **87,** 11242–11248 (2015).
28. Marginean, I., Nemes, P. & Vertes, A. Astable regime in electrosprays. *Phys. Rev. E* **76,** 026320 (2007).
29. Whelan, M. *et al.* Determination of anthelmintic drug residues in milk using ultra high performance liquid chromatography-tandem mass spectrometry with rapid polarity switching. *J. Chromatogr. A* **1217,** 4612–4622 (2010).
30. Nazari, M. & Muddiman, D. C. Polarity switching mass spectrometry imaging of healthy and cancerous hen ovarian tissue sections by infrared matrix-assisted laser desorption electrospray ionization (IR-MALDESI). *Analyst* **141,** 595–605 (2016).
31. Harris, G. A., Kwasnik, M. & Fernandez, F. M. Direct analysis in real time coupled to multiplexed drift tube ion mobility spectrometry for detecting toxic chemicals. *Anal. Chem.* **83,** 1908–1915 (2011).
32. Allen, S. J., Schwartz, A. M. & Bush, M. F. Effects of polarity on the structures and charge states of native-like proteins and protein complexes in the gas phase. *Anal. Chem.* **85,** 12055–12061 (2013).
33. Wampler, F. M., Blades, A. T. & Kebarle, P. Negative ion electrospray mass spectrometry of nucleotides: ionization from water solution with SF_6 discharge suppression. *J. Am. Soc. Mass Spectrom.* **4,** 289–295 (1993).
34. Monge, M. E., Harris, G. A., Dwivedi, P. & Fernandez, F. M. Mass spectrometry: recent advances in direct open air surface sampling/ionization. *Chem. Rev.* **113,** 2269–2308 (2013).
35. Verbeck, G., Hoffmann, W. & Walton, B. Soft-landing preparative mass spectrometry. *Analyst* **137,** 4393–4407 (2012).
36. Tyo, E. C. & Vajda, S. Catalysis by clusters with precise numbers of atoms. *Nat. Nanotech.* **10,** 577–588 (2015).
37. Johnson, G. E., Colby, R., Engelhard, M., Moon, D. & Laskin, J. Soft landing of bare PtRu nanoparticles for electrochemical reduction of oxygen. *Nanoscale* **7,** 12379–12391 (2015).
38. Ouyang, Z. *et al.* Preparing protein microarrays by soft-landing of mass-selected ions. *Science* **301,** 1351–1354 (2003).
39. Ju, J., Yamagata, Y. & Higuchi, T. Thin-film fabrication method for organic light-emitting diodes using electrospray deposition. *Adv. Mater.* **21,** 4343–4347 (2009).
40. Bender, F., Wachter, L., Voigt, A. & Rapp, M. Deposition of high quality coatings on saw sensors using electrospray. *Proc. IEEE Sensors* **1,** 115–119 (2003).
41. Li, A. *et al.* Using ambient ion beams to write nanostructured patterns for surface enhanced raman spectroscopy. *Angew. Chem. Int. Ed.* **53,** 12528–12531 (2014).

Acknowledgements

This work was jointly supported by the National Science Foundation (NSF) and the NASA Astrobiology Program, under the NSF Center for Chemical Evolution, CHE-1504217. Research was also supported by the US Department of Energy, Office of Basic Energy Sciences (award DE-FG02-07ER46394) and the National Science Foundation (DMR-1505319).

Author contributions

A.L., Y.Z., F.M.F. and Z.L.W. conceived the idea, discussed the data and prepared the manuscript. A.L. and Y.Z. performed electrical measurements. Y.Z. fabricated the TENGs. A.L. performed mass spectrometry experiments. H.G. provided assistance with the experiments.

Additional information

Supplementary information is available in the online version of the paper. Reprints and permissions information is available online at www.nature.com/reprints. Correspondence and requests for materials should be addressed to Z.L.W. and F.M.F.

Competing financial interests

The authors declare no competing financial interests.

Methods

Fabrication and operation of TENGs. The static part of the CS-TENG assembly was constructed by attaching a copper foil to an acrylic board (45×45 mm^2). The movable CS-TENG part (45×45 mm^2) was fabricated by physical vapour deposition of 0.1 μm Cu on a 50-μm-thick fluorinated ethylene propylene (FEP) film, also supported on acrylic. The static part of SF-TENGs consisted of Cu film deposited onto FEP as two 75×60 mm^2 rectangles separated by a 75×1 mm^2 uncoated rectangular region, mounted on acrylic. The movable SF-TENG part was made of a Cu foil (55×65 mm^2) mounted onto an acrylic board. To operate the TENG, the movable parts were mounted either on a linear motor, or on a UR5 robotic arm (Universal Robots Inc.), while the static part was fixed onto a stage. They are mounted facing each other so that the two metal layers are separated by the FEP layer (Fig. 1). For CS-TENGs, the movable part was actuated with a full separation displacement of 12.2 mm, acceleration of 2 m s^{-2}, speed of 1 m s^{-1}, a delay time of 0.5 s at full contact, and a delay time of 5 s at full separation. For SF-TENGs, the movable part was 'slid' between the two positions coinciding with the two Cu-coated regions of the static part, with a travel distance of 60 mm. The slide time was 0.5 s, and a delay time of 2–10 s was applied after the movable part reached each square static Cu electrode. Higher-frequency pulses were generated by rapidly switching the direction of the sliding motion at defined slide times, without any delay time. The performance of the devices was stable throughout the experiments for at least 9 months, or ~8,000 cycles.

Ion source, circuits, voltage and charge measurement. NanoESI emitters were fabricated by pulling borosilicate glass capillaries using a p97 puller (Sutter Instrument). A Au wire or a 50-nm-Au-coated layer were used to provide electric contact to the sample solutions loaded in the nanoESI emitter. For LOD experiments, glass tips with conductive coating were purchased (Econo 12, New Objective) and used without further modification. For plasma ionization, a stainless steel acupuncture needle (Ø0.25 × 13 mm, Millennia) was used to induce corona discharges. The corona discharge needles and nanoESI emitters were connected to one of the electrodes of the TENG device, either directly or through GΩ resistors (Ohmite). A bridge rectifier composed of four diodes (Digikey, #1N4004) was used to generate single-polarity pulses when needed. NanoESI emitters were placed so that their tips were 5–10 mm away from a grounded plate or the mass spectrometer's inlet. For atmospheric pressure chemical ionization experiments the discharge needle's sharp tip was placed 1.5 mm away from the mass spectrometer inlet. The spray plume was visualized using an Ablegrid digital microscope (B014CU4QAI, Amazon) under orthogonal illumination by a laser pen (405 nm, 5 mW). A Keithley 6514 programmable electrometer under LabView control was used to measure the transferred charge or the voltage. When the electrometer was in its voltage measurement mode, it is referred to as the 'voltmeter' in this Article. A high-voltage power supply (PS350, Stanford Research Systems) was used to probe the nanoESI onset voltages. Note that when a voltmeter was connected in parallel with the ion source, a V_{OC} reading of 300 V was obtained and no ionization was observed. This is due to the fact that a significant amount of charges was being consumed by the voltmeter, and suggests that the true TENG peak voltage output could be significantly higher than that that measured by directly using voltmeter (Supplementary Fig. 1) (due to the internal capacitance of the voltmeter, the measurement itself consumes charge from the TENG and lowers the voltage). Using a series of ESI emitters with different onset voltages (by varying the emitter tip's inner diameter and tip-to-ground distance), we estimated the V_{OC} of the CS-TENG and the SF-TENG to be ~1,600 V and >2,000 V, respectively (Supplementary Fig. 2 and Supplementary Table 1). These values were confirmed by other independent measurement methods (Supplementary Fig. 3, and Supplementary Tables 2 and 3). The measured capacitance of 301 pF for the voltmeter (Supplementary Fig. 5) is much larger than the electrospray ion source, resulting in unwanted charge consumption during V_{OC} measurements. This is why the V_{OC} of TENGs had been previously measured (Supplementary Fig. 1) only in the 300 V range.

Mass spectrometric analysis. A Q-Exactive hybrid quadrupole-Orbitrap mass spectrometer (Thermo Scientific) was used to analyse the generated ions with the following parameters, unless otherwise noted: capillary temperature 150 °C, S-lens radio frequency level of 40, maximum injection time of 15 ms, the automatic gain control (AGC) target set at 1×10^6, and a mass resolution of 17,500. Tandem MS experiments were carried out with an isolation window of 1.5 Da, a normalized collision energy of 35 and the AGC target set at 5×10^5.

TENG spray deposition. The target surfaces used in the deposition experiments included indium tin oxide (ITO)-coated glass slides (CG-40IN-S115, Delta Technologies), 130-μm-thick micro cover glass slides (Cat. # 48404, VWR) and 68-μm-thick polyimide tape (Cat. #5433, 3M). Conductive target surfaces were grounded. Insulating surfaces were mounted on top of grounded ITO or metal plates. The surfaces were positioned 5–10 mm away from the tip of the nanoESI emitters. 10 mM dye solutions were loaded in the emitter. Empty transmission electron microscopy grids or a stainless steel mesh with 200 μm perforations were used as masks when needed. The target surface was placed on a moving stage (OptiScan ES111, Prior Scientific) that allowed its position to be controlled relative to the emitter.

Data availability. The data that support the plots within this paper and other findings of this study are available from the corresponding authors upon reasonable request.